Pierre Auger Observatory hybrid events: design, analysis, and preliminary results

M. A. DuVernois and C. Song for the Pierre Auger Collaboration*

School of Physics and Astronomy, University of Minnesota, Minneapolis, MN 55455, U.S.A

ABSTRACT

The Pierre Auger Project is an international effort to make a high statistics study of cosmic rays at the highest energies. To obtain full sky coverage two nearly identical air shower detectors will be constructed, one to be placed in the Northern Hemisphere and one in the Southern Hemisphere. Each installation will have an array of about 1,600 particle detectors spread over 3,000 km^2. Atmospheric fluorescence telescopes placed within and on the boundaries of the surface array will record showers that strike the array. The two air shower detector techniques working together form a powerful, hybrid, instrument for these studies. The results from both air fluorescence and surface detectors, on their own, have been quite notable, but are also notable in their disagreement with each other. Hence the concept of an experiment unifying the two approaches to the highest-energy cosmic rays. It is the design of the hybrid nature of the experiment, the analysis of events with hybrid information, and some preliminary results that will be discussed here.

Keywords: Cosmic rays, extensive air showers, detectors

1. INTRODUCTION

Cosmic rays have a long history, starting with Victor Hess at the turn of the last century, which need not be repeated here. We are concerned with the highest energy cosmic rays which are observed, indirectly, through their cascading air-showers produced by nuclear interactions in the atmosphere. Since Pierre Auger discovered extensive air showers (EAS),[1] physicists have observed high energy cosmic rays up to over 10^{20} eV. The origin and propagation of such cosmic rays are not obvious. At the highest energies, some of these events are above the predicted cut-off due to photo-pion production off of the microwave background photons. Interpretations do vary, but regardless of origin, such energetic particles are of considerable interest.

Construction has begun on the southern site of the Auger Observatory located in the Province of Mendoza, Argentina. The scientific goal of the Pierre Auger Observatory is to discover and understand the source or sources of cosmic rays with energies exceeding 10^{19} eV. The method measures the energy spectrum, the arrival directions, and the nuclear composition of these particles. A detailed and thorough study of cosmic rays above 10^{20} eV is particularly important toward this end. To achieve these goals it is necessary to measure the energy spectrum, to accumulate substantially more events than previous and current experiments, to determine accurately the arrival directions of the particles and to use the characteristics of the events to estimate the masses of the primaries. The experiment measures these properties of extensive air showers. Historical references can be found in Ref. [2–5] and further details of the Auger Observatory in Ref. [6–8]

A unique feature and strength of the Auger Observatory is that it is a hybrid detector consisting of a surface detector and an atmospheric fluorescence detector. This is in contrast to previous detectors which used only one technique and suffered from difficult to understand systematics. The duty cycle of the surface detector should be nearly 100% whereas the fluorescence detector duty cycle may be only 10%. The hybrid data set obtained when both detectors are working together will be especially important for evaluating the systematics of both detectors. It will also provide an energy spectrum with small energy uncertainties. The hybrid data set will also provide the best evaluation of the primary particle composition utilizing all of the known parameters that are sensitive to the primary particle type. The hybrid data set will be limited in statistics, however. At the highest energies, the spectrum and composition measurements will rely primarily on the surface detector alone. The correlation of hybrid and surface detector-only analyses in the high-statistics regime will justify the reliance on surface detector-only data at the highest energies.

*Pierre Auger collaboration list at http://auger.cnrs.fr/collaboration.html.

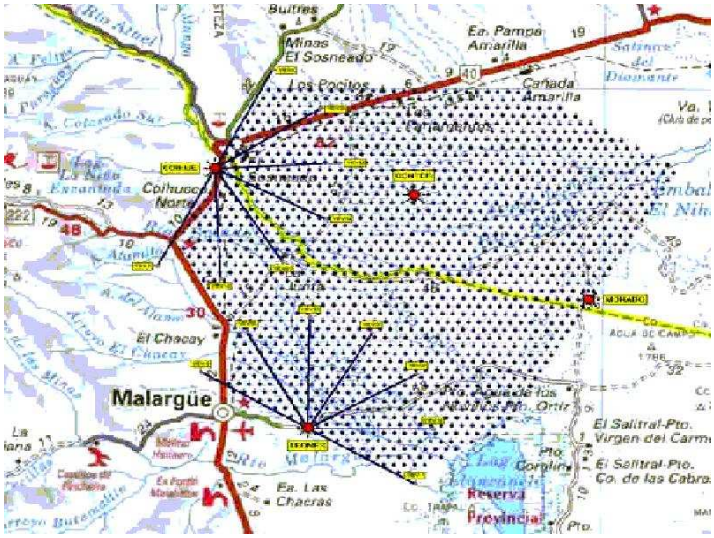

Figure 1. The layout of the Pierre Auger southern hemisphere site. Fluorescence detectors, surface detectors, and local terrain are indicated. The central Auger campus is located in the town of Malargue.

2. PROJECT DESCRIPTION

2.1. Observatory Site

The southern site of the Auger Observatory is located in western Argentina in the Province of Mendoza. The area covered by the array is an ancient lake bed sufficiently flat to accommodate line of sight radio communications between each detector station and one of four antenna towers located adjacent to the fluorescence detector buildings. On the boundary of the surface array, elevated surface features have been selected for the fluorescence buildings that elevate them above possible ground fog. Figure 1 shows the array and the positions of the four fluorescence detector stations, the layout of the 1,600 surface detectors, and the local political and geographical divisions.

The construction of the southern site of Auger Observatory was planned to take place in two steps. The first two years were devoted to the Engineering Array (EA) followed by three years to complete full observatory construction. The EA consists of 40 prototype surface detector stations and two-prototype fluorescence telescopes. The two fluorescence detector prototypes overlook the prototype surface array. Construction of the EA began in January of 2000. Data collection continues with the EA as production quantities of all components and systems are ordered and arrive in Mendoza Province. The objective of the EA was to evaluate the performance of every component and system in the field before proceeding to full production and deployment. Full construction and deployment are expected to take three years. After the first year of construction, routine data taking will begin. At that time, the Auger Observatory will be the world's largest air shower array.

2.2. Surface array

The role of the surface array is to measure the lateral density and time distribution of particles in the shower front at ground level. These shower quantities are correlated with the energy, the direction, and to some extent with the nature of the primary particle. The detector performance in measuring these parameters defines the physics performance of the surface array. The resulting detector parameters have been studied using shower and detector simulations as well as with the experience gained with earlier surface arrays. The conclusions of these studies are detailed in the Auger Design Report .[7] It should be noted that, since the Design Report was written, the physics goals have been enhanced by the prospect of neutrino detection from large zenith angle showers.

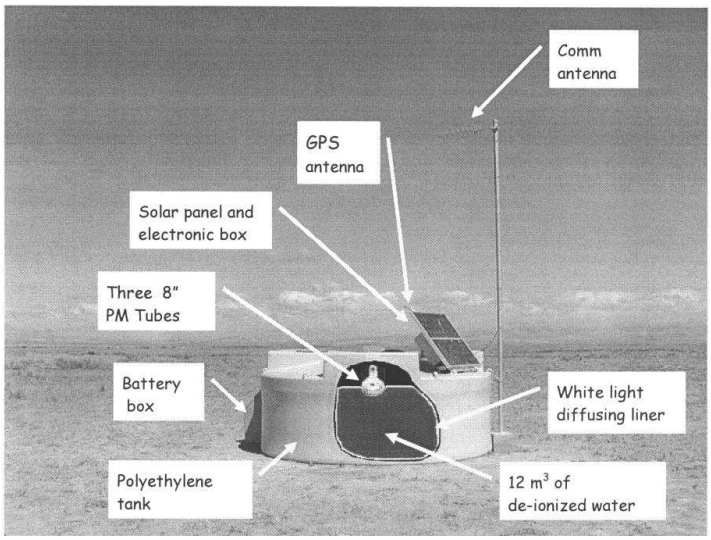

Figure 2. The vital parts of a surface detector (an engineering array tank, part of the 2001-2002 hybrid data-taking operation, is pictured here)—one of 1,600 to be placed in the field. From the top: a radio antenna for the TDMA communication system, GPS antenna for absolute and relative timing, solar panel for power systems, electronics box (in the engineering array this is behind the solar panel as pictured, in production it will drop under a top hatch cover), 8" hemispherical PMTs observing the water volume, the water volume itself, a box containing 24VDC deep-cycle batteries and charge controller, and the rotationally molded high-density polyethylene (HDPE) tank with tyvek liner.

The main choices and the basic detector parameter definitions were also already justified in the Design Report. Uniform sky coverage is required for anisotropy studies and the observatory will consist of two sites, both located at about 30 degree latitudes, North and South. The size of each array is driven by the goal to collect high statistics above the predicted GZK cut-off. The required limiting aperture requires the instrumentation of an area of 3,000 km^2 per site. The spacing of 1.5 km between detection stations is defined by the requirement of full detection efficiency above 10^{19} eV and of a good sampling of the lateral density distributions. The low density of particles ($\sim 1/m^2$) to be measured with good statistical precision imposes a sampling area of ~ 10 m^2.

The water Cherenkov detection technique has been selected mainly from cost considerations but also because of its own virtues: the water tank offers a natural way to optimize muon pulse heights with respect to the electromagnetic component. Because of its large lateral cross-section it offers a good sensitivity to large zenith angle showers. The experience from the Haverah Park array, where water Cherenkov detectors of similar area and height were used, backs this choice. Thus, the surface array will be comprised of 1,600 water Cherenkov detectors spaced by 1.5 km on a triangular matrix and instrumenting an area of about 3,000 km^2.

Each detector consists of a cylindrical, opaque tank having a diameter of 3.6 m and a water height of 1.2 m. The water is contained in a sealed bag or liner that prevents contamination, provides a barrier against any remaining external light, and diffusely reflects the Cherenkov light emitted in the water. Three large diameter ($\sim$20 cm) hemispherical photomultipliers (PMTs) are mounted facing down and look at the water through three sealed windows that are an integral part of the liner. The liner also provides filling ports and possibly an additional sealed window hosting an LED calibration system. The PMTs are enclosed in housings to further protect them from external light. On the outside, the tank has supports for solar panels providing the energy supply and for the communication system and GPS antenna. A battery is contained in a box attached to the tank. See Figure 2 for a schematic overview of a single Surface Detector (SD) tank in the field.

2.2.1. Energy

The shower energy is obtained by assessing the size of the shower, through the determination of the density at a particular radius of 600 to 1000 m. The measured densities are affected by fluctuations from different origins:

Zenith angle	protons/iron		Unconverted photons
	All energies	$E > 10^{20}$ eV	
20°	1.1°	0.6°	4.0°
40°	0.6°	0.5°	2.5°
60°	0.4°	0.3°	1.0°
80°	0.3°	0.2°	1.0°

Table 1. Direction error of surface detector (space angle containing 68% of the events). Converted photons are easy to identify at the 10% level by shower front curvature, rise time and muon content.

statistical fluctuations in the measured density and experimental uncertainties on the shower direction; large physical fluctuations in the shower longitudinal development that lead to shower-to-shower density fluctuations. Furthermore, the relation between the measured densities and the primary energy is obtained using interaction models and shower simulations. A corresponding systematic uncertainty from model dependence is to be assessed when considering energy measurements. Using the fraction of events that the observatory will detect in the hybrid mode, detailed studies of the shower longitudinal development and cross-calibration will be possible, and we expect to reduce the model dependence of the energy determination by the surface detector alone. The resulting energy resolution is 12% RMS for all events and 10% for events above 10^{20} eV.

It is important to reduce the experimental uncertainty in the measured density as much as possible. At high energy, about 6% of the statistical uncertainty arises from the measurement errors and the rest are from the shower-to-shower fluctuations. The relative error in the particle density measurement at 1,000 m from the core should be less than 20%. The muon flux at this distance is of the order of $1/\mathrm{m}^2$ at 10^{19} eV. Hence, a minimum sampling surface of 10 m^2 is required.

2.2.2. Angular resolution

The direction of the primary is inferred from the relative arrival times of the shower front at different surface detectors. A weighted least squares fit is applied to the station triggering times. Fitting the station signal densities to the expected lateral distribution makes refined core location estimation. For the surface array alone, we expect an angular precision of 0.6 degrees for energies $>10^{20}$ eV. This angular accuracy is quoted for the opening angle containing 68% of the reconstructed directions. The angular resolution improves rapidly with zenith angle and energy because of the larger trigger time differences and the greater number of triggered stations. Reconstruction accuracy for the surface array is summarized in Table 1.

2.2.3. Composition

Heavy primary particles tend to produce more muons and fewer electromagnetic particles than do lighter primaries, when measured at the same total energy. Iron and proton showers may be differentiated using surface detector data alone through the analysis of the ratio of muons to electromagnetic particles, as well as through the arrival time distribution of particles in the shower front. Photons and neutrinos leave very characteristic signatures such as shower front curvature. The height of the water Cherenkov detector is defined to optimize the muon pulse height. A vertical distance of 1.2 m of water is sufficient to absorb 85% of the incident electromagnetic shower energy at core distances >100 m, and gives a signal proportional to the energy of the electromagnetic component. Muons passing through the tank generate a signal proportional to their geometric path length inside the detector and rather independent of their zenith angle and position. The number of photoelectrons per PMT corresponding to a vertical muon is in excess of 30 photoelectrons. Muonic content, rise-time and time profile, are extracted from the measured PMT signal waveforms. This information provides a multivariate handle on the composition of the population of primary cosmic rays. Details of techniques for this type of analysis are still under development.

2.2.4. Aperture

The required limiting aperture of the ground array for zenith angles $< 60^\circ$ is 7,350 km^2-sr for each hemisphere's detector. The detection efficiency at the trigger level should reach 100% for energies above 3×10^{18} eV. This aperture is achieved by covering an area of 3,000 km^2 per site. The spacing between the detector stations is the result of a compromise between cost considerations and the energy threshold (low enough to insure a good overlap with existing data) as well as a sufficient sampling of the particle density away from the shower core, and of the shower front timing in several places. A minimum of 5 stations triggering at 10^{19} eV fixes the maximum spacing to $\sim$1.5 km. The number of triggered stations for energies $>10^{20}$ eV is $\sim$15 stations. This adds up to a total number of 1,600 detector stations per site. The surface arrays in both hemispheres will provide data from a nearly uniform celestial exposure. This enables a straightforward search for excess from discrete sources and also a sensitive large-scale anisotropy analysis.

If events above 60 degrees can be effectively analyzed, as appear likely, the above aperture will increase by about 50%. The efficiency for detecting events is shown in Table 2.

2.3. Fluorescence Detector

The longitudinal shower profile measured by the fluorescence detector (Figure 3) provides a nearly model-independent measure of the electromagnetic shower energy. The primary energy can be estimated as 10% greater than the electromagnetic shower energy, and simulations show that this estimate is systematically in error at most by 5%, regardless of the type of primary particles. The number, distribution and resolution of the fluorescence telescopes was determined by the requirement that showers be visible over the entire surface array at energies above 10^{19} eV. The Auger Observatory will have a total of 30 telescopes located in four enclosures located within or on the edge of the surface array. The Auger fluorescence detector is expected to operate always in conjunction with the surface detector. This is known as the hybrid mode. Its primary purpose is to measure the longitudinal profile of showers recorded by the surface detector whenever it is dark and clear enough to make reliable measurements of atmospheric fluorescence from air showers.

The fluorescence detector requirements are driven by X_{max} resolution that is necessary for evaluating the composition of the cosmic ray primaries. The X_{max} resolution (uncertainty in atmospheric depth where a shower reaches maximum size) should be small compared to the (approximately 100 g/cm^2) difference expected between X_{max} for a proton shower and for an iron shower of the same energy. Moreover, the experimental resolution should not significantly increase the spread of values for any one component of the composition by itself. The width of the expected X_{max} values for any nuclear type decreases with mass A and the distribution of iron X_{max} values has an RMS spread of approximately 30 g/cm^2. We will therefore require that the experimental X_{max} resolution be no greater than 20 g/cm^2.

An accurate longitudinal profile (achieving 20 g/cm^2 X_{max} resolution) requires good geometric reconstruction of the shower axis. At large zenith angles, a small error in zenith angle causes a significant error in atmospheric slant depth. Averaging over the range of hybrid shower zenith angles (0-60 degrees) leads to a

Energy (eV)	Efficiency	
	Zenith angle $< 60^\circ$	Zenith angle $> 60^\circ$
1×10^{18}	0.00	0.00
3×10^{18}	0.30	0.50 @ 70°, 0.75 @ 75°, 0.80 @ 80°
1×10^{19}	0.98	1.00
3×10^{19}	1.00	1.00
1×10^{20}	1.00	1.00

Table 2. Energy efficiency of the surface detector acting independently. Low-energy cutoff is due to minimum number of tank hit required to form software trigger at the central station—this has been relaxed during the engineering array operation. Events at >60 degrees can be efficiently triggered on due to the water Cherenkov tank vertical extent. Each tank's angular geometric acceptance is roughly constant.

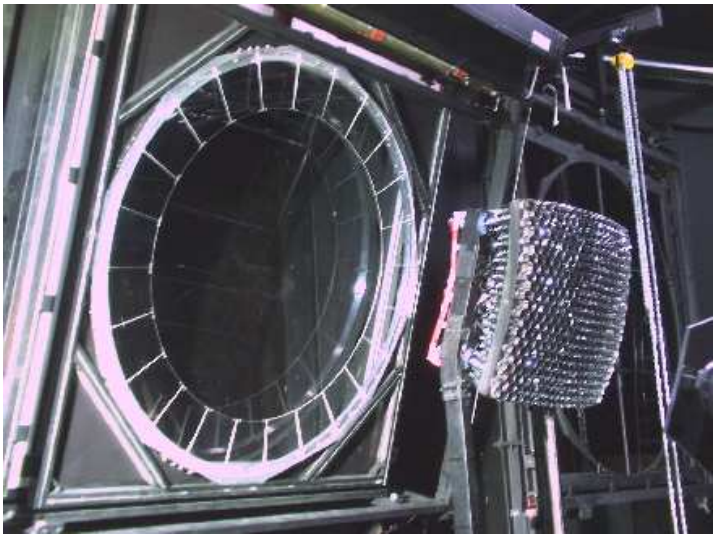

Figure 3. A photo of one of the prototype Auger fluorescence detectors installed at the Los Leones site (south of the Auger surface array). This prototype, and the one to its immediate right, provided the fluorescence data for the engineering array hybrid runs of 2001 and 2002.

rule of thumb that an error of one degree in zenith angle leads to an error of 20 g/cm^2 in X_{max}. The angular resolution of the hybrid showers must therefore be significantly better than 1 degree, since other uncertainties also contribute to the X_{max} uncertainty.

The longitudinal profile of each shower must be well measured in order to determine the depth of maximum to 20 g/cm^2. In particular, the profile will be well enough measured that the profile integral (proportional to the total shower electromagnetic energy) will have less than a 10% fitting uncertainty contributing to the shower energy uncertainty. Good energy resolution is therefore implicit in the X_{max} resolution requirement. Hybrid performance is shown in Tables 3. The errors shown in Table 3 are statistical only.

2.3.1. Aperture

Aperture and detector efficiency are especially important for fluorescence detectors since their acceptance is a function both of energy and atmospheric conditions. For Auger, the surface detector constrains, and helps determine, this acceptance for events which fall within the array—that is, the hybrid events. Simulations have been performed to calculate the triggering aperture of the FD baseline design, with the arrangement of eyes shown in Figure 1. The simulations require a hybrid trigger (that is, triggers in at least one FD eye and at least two surface detectors). The design requirement is that the efficiency be near 100% at 10^{19} eV. In this figure it is clear that the FD will have a large stereo aperture at energies well above the threshold. Because we have access to SD timing information, stereo views are not vital for geometric reconstruction of the shower axis, but

	$\Delta E/E$ (%)			ΔX_{max} (g/cm^2)			Δdir ($^\circ$)		
Confidence limits	50%	68%	90%	50%	68%	90%	50%	68%	90%
$E = 10^{18}$ eV	9.5	13	21	21	38	74	0.50	0.73	1.55
$E = 10^{19}$ eV	4.5	6.5	13	14	25	62	0.35	0.51	1.10
$E = 10^{20}$ eV	2.5	5.5	17	12	24	69	0.35	0.51	0.90

Table 3. Hybrid resolution in terms of energy resolution, X_{max} uncertainty, and angular resolution on the sky. Confidence limits are set median energy and impact parameters. High zenith angle and hits near the array perimeter produce more highly asymmetric error distributions.

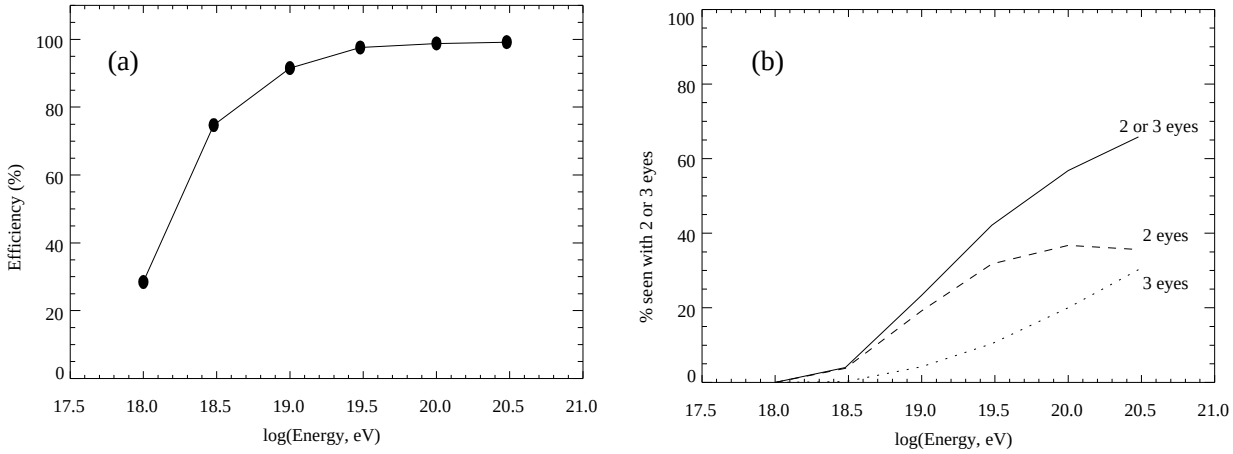

Figure 4. Left panel: The hybrid triggering efficiency as a function of energy for showers (with zenith angles less than 60 degrees) falling at random positions within the surface array boundary. At lease one fluorescence eye and two surface detectors are required to trigger. Note the acceptable aperture at energies lower than the nominal turn-on energy at 10^{19} eV. The triggering aperture can be obtained by multiplying the efficiency by 7,375 km^2-sr. Right panel: The fraction of events triggering more than one fluorescence station. This is the traditional multi-"eye" detection mode from Fly's Eye and HiRes experiments. It is an accidental consequence of demanding good hybrid coverage and allows yet another cross-check to the fluorescence atmospheric corrections.

stereo views will assist in cross checks of our atmospheric transmission measurements. Also stereo triggers will yield some well-measured showers (at large zenith angles or with cores outside the array) that are not recorded by the surface array. There will be a large set of hybrid showers with energies below 10^{18} eV. The number of such showers will exceed the number recorded with energies above 10^{19} eV, even though the aperture is not that of the entire surface array. The FD measures such showers only if they land within some radius of one of the eyes, where the radius is energy dependent.

The arrangement of four eyes at the Argentinian site reduces our dependence on a precise knowledge of light transmission through the atmosphere. The mean impact parameter from the closest triggering eye is 13 km at 10^{19} eV, compared with the effective Rayleigh scattering attenuation length (averaged over all light paths) of 19.5 km at 350 nm.

2.3.2. Angular resolution

As discussed above, the angular resolution of the detector must be small compared with 1 degree, and the reference design will achieve an angular resolution of 0.5 degrees. There are two aspects of the angular resolution: the shower-detector plane determination and the angle of the shower axis within that plane. The shower-detector plane is determined by the set of pixels that see the shower axis. The need to resolve the shower-detector plane to better than 0.5 degrees has led to the constraint that the pixel size cannot be larger than 1.5 degrees in effective diameter. Determining the shower axis within the track-detector plane is done exclusively with timing information. The angular velocity of the shower front image moving through the FD field of view does not uniquely determine the shower axis. It does reduce the 2-parameter family of lines in the shower-detector plane to a 1-parameter family of possible axes. Each hypothetical axis makes a specific prediction for the arrival time of the shower front at each surface detector. The measured arrival times at one or more surface detectors thereby determine the correct shower axis. The need for good timing information is a primary reason for using sampling ADC electronics rather than simply recording a charge integral for triggering pixels. The ADC trace in each pixel allows an accurate determination of the time at which the shower front passed the center of the pixel. Analytic arguments and simulations show that time slices of 100 ns will yield the necessary timing accuracy to achieve the required angular resolution.

No of trigger tanks	1	2	3	4	≥5	All
Dec. 2001	17	4	-	-	-	21
Jan. 2002	18	4	-	1	-	23
Feb. 2002	7	2	2	1	-	12
Mar. 2002	7	6	4	-	4	21
Sum	49	16	6	2	4	77

Table 4. Triggered events for the engineering array in coincidence with the two prototype fluorescence detectors in Los Leones for December 2001 through March 2002. The low numbers are due to FD live-time, SD elongated layout, and SD operations. These events are useful internally to Auger, but do not represent science results..

3. ANALYSIS

We focus on the hybrid analysis of the events taken with the 40-tank SD engineering array and the prototype fluorescence telescopes. To do so we must consider some aspects of both the SD energy and geometric reconstruction as well as the fluorescence reconstruction.

3.1. Hybrid Events

From December 2001 through March 2002, the Southern Auger Observatory took hybrid data—triggers in both FD and SD. After selections, 77 events, summarized in Table 4, were kept for analysis. This small number was due to the geometry of the EA (elongated due to surface topography) and tank operations. By the end of the hybrid run, the surface and fluorescence detectors were working at near 100% efficiency (SD tanks on 100% of the time and FD telescopes operating on clear-moonless nights). The total number of hybrid events is too small to deduce physical meanings from data, but these events are very useful means to check our analysis software and to develop new reconstruction methods.

3.2. Geometry Reconstruction

First of all, the axis of the air shower should be determined to calculate atmospheric depth of a shower track. Eventually, raw electrical signals are interpreted into useful information such as longitudinal shower profile for FD and shower lateral distribution at ground level for SD. To reach this point, we go through several steps.

The first step is to determine arrival direction and core location at ground level. This can be done easily by using SD measurements. The position of the core at ground may be approximated as an average of the station coordinates with suitable weights, for example $w_i = \sqrt{S_i}$ to define $x_{av} = \sum w_i x_i / \sum w_i$ and $y_{av} = \sum w_i y_i / \sum w_i$; the precision is of the order of 100 m.

A good approximation of the direction may be found using the first time slot above a given threshold (typically 5 photoelectrons), t_0, of the three stations with highest integrated signals S (more precisely: the highest two, plus the next highest one which is not aligned with them). Assuming a planar front moving at speed c, we can write:

$$t_0 = T_0 - (ux + vy + \sqrt{1 - u^2 - v^2}z)/c \tag{1}$$

with $u = \sin\theta\cos\phi$ and $v = \sin\theta\sin\phi$, hence 3 independent equations to determine 3 unknowns T_0, u and v. The direction cosines (u, v) are obtained from the t_{0i}'s of all stations through a least squares fit of the front plane:

$$\chi^2 = \sum_i \frac{\Delta t_i^2}{\sigma_i^2} \tag{2}$$

with

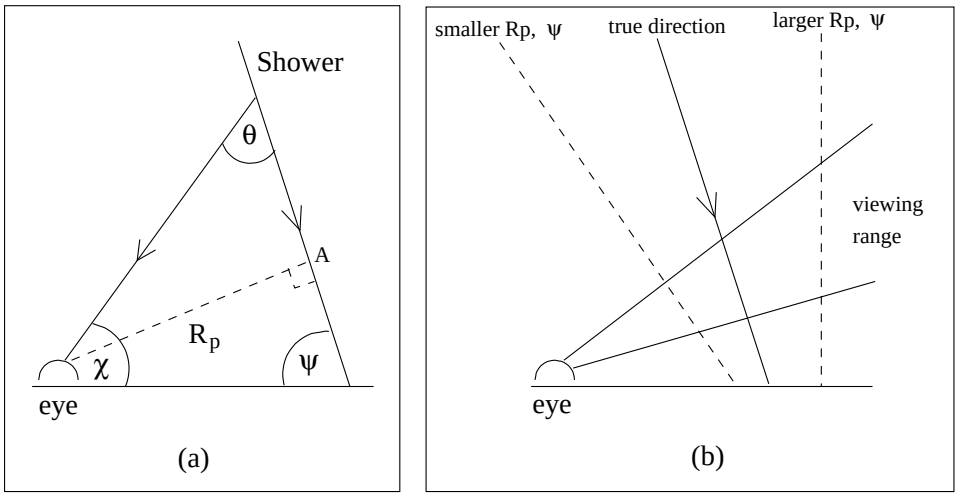

Figure 5. The shower-detector plane (SDP) geometry detailed. In hybrid events this plane is further constrained by the surface detector hits and surface detector reconstruction of the shower.

$$\Delta t_i = t_{0i} + \{u(x_i - x_{av}) + v(y_i - y_{av}) + \sqrt{1 - u^2 - v^2}\, z_i\}/c \tag{3}$$

T_0 is an additional free parameter, which should be close to the arrival time of the core at the ground; however it is biased because of the curvature of the front. The front curvature may be parameterized with a paraboloidal parameterization.

By the way, the first step on FD side is the electronic and optical calibration, where FADC traces are converted to light fluxes seen by pixels, in units of 370 nm-equivalent photons impinging on the mirror diaphragm per 100 ns time bin. The next step is the determination of the orientation of the shower axis in space. The Auger fluorescence detectors are primarily designed to view showers in coincidence with the surface array. Here the reconstruction of the geometry of the shower axis will use timing and light amplitude information from the FD together with timing data from the SD.

The first step to determine shower core location and direction with single eye is the determination of the plane containing the shower axis and the center of the eye. This shower-detector plane (SDP) fit uses tube pointing directions, together with signal integrals. Tube timing information is not used at this stage, except to discard noise tubes. Trial planes are compared with the pointing directions of fired phototubes, with the fit weighted by the signal amplitudes. Once the SDP is determined, the trigger times of the tubes are used to determine the orientation of the axis within that plane. For a given geometry (Figure 5), the arrival time of light at a tube viewing the axis at an angle θ_i is

$$t(\theta_i) = \frac{R_p}{c} \tan(\frac{\theta_i}{2}) + t_0 \tag{4}$$

where t_0 is the time at which the shower passes at the closest point to the detector and R_p is an impact parameter. There is a problem with these timing fits, especially for short tracks. The range of θ_i sampled is not large enough to detect significant curvature in the tangent function in the above equation. Unfortunately, this leads to ambiguity in the fit, with a family of possible (R_p, ψ) combinations.

This ambiguity can be resolved by using other information, for example, a SDP from another detector, or information from a ground array. The most promising ground parameter is the arrival time of the shower at the ground. It is obvious that if all eye and ground array times are measured with a common clock, then the ground array times will constrain the timing fit within the SDP. The hybrid geometry reconstruction proceeds in the following way. The SDP is determined by using fluorescence information only. Typically, the plane orientation

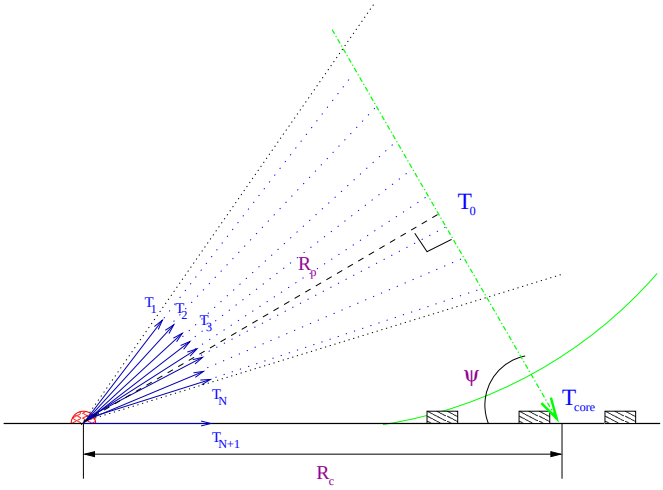

Figure 6. Hybrid geometry in the Auger Observatory. Surface Detector triggers form effective additional fluorescence pixels near ground level. This incorporates SD data directly into the FD reconstruction. Optimized methods of combining the data are under investigation.

is known to better than 0.25°, which is corresponds to a distance of a most 60 m on the ground at a distance of 15 km. The, it is assumed that the shower core is contained on the the line forming the intersection of the SDP and ground. The timing fit is performed, minimizing a χ^2 which includes the standard fluorescence timing term and an array timing term.

The fluorescence timing term is given by

$$\chi_1^2 = \frac{N_i}{\sum pe_i} \sum_i \frac{(t_i - t_{expected})^2}{\sigma_i^2} pe_i \tag{5}$$

where t_i is the estimate of the pulse mid-point time, and σ_i is the mid-point time uncertainty for each tube. The elements of the sum are weighted by pe_i, signal in each tube. The sum is multiplied by N_i, the number of firing tubes, to give the appropriate weight to this term of the χ^2 when the array component is added. By the way, the array component of the χ^2 may be given by

$$\chi_2^2 = \sum_i \frac{(t_i - t_{expected})^2}{\sigma_i^2} \tag{6}$$

where

$$\sigma_i = \frac{\sigma_i^{'}}{\sqrt{n_i}} \tag{7}$$

where the sum is over all detectors with particle counts greater than 10 particles. t_i is the mean arrival time of the particles at each detector, $\sigma_i^{'}$ is the dispersion in the particle arrival time, and n_i is the number of particles detected. Finally, the final χ^2 minimization is performed on the linear sum of the fluorescence and ground array components, with the ground array component. That is,

$$\chi^2 = \chi_1^2 + \chi_2^2 \tag{8}$$

Alternatively, we can treat both detectors as parts of single detector. As illustrated in Figure 6, SD provides additional information about core pointing direction from FD, and then FD time fit determines axis within the SDP while the axis is constrained by core location obtained by SD. This constrained fit will work well especially for short track events. In this case, we do not need to deal with two different χ^2s. However, both FD and SD clocks should be synchronized. This method has been being studied.

3.3. Energy Determination

Once a shower axis is determined, FD can calculate the number of charged particle as a function of atmospheric depth and SD can measure the particle density as a function of distance from shower axis at ground level. We determine the shower longitudinal profile by using the geometrical information and the received light flux, as well as information on the atmospheric transparency and the fluorescence yield from shower particles. Finally, the longitudinal profile is interpreted to extract the primary particle energy, and mass composition parameters like X_{max}.

To determine energy by FD information, we integrate the longitudinal profile of charged particle to obtain the total ionization energy loss:

$$E_{cal} = \alpha \int_0^\infty N_{ch}(X) dX, \tag{9}$$

where $N_{ch}(X)$ is the number of charged particles at depth X and α is 2.19 MeV/g/cm^2.[9] The energy must be corrected by missing energies channeled into high energy muons, neutrinos and nuclear excitations. Based on air shower simulation, the correction can be parameterized as:

$$E_{cal}/E_o^{FD} = 0.959 - 0.082\ E_{cal}^{-0.150} \tag{10}$$

where E_o^{FD} is the primary energy and E_{cal} is the calorimetric energy derived from Eq. (10). Eq. (10) is valid for $3 \times 10^{16} < E_o^{FD} < 10^{20}$ eV. The analysis shows that different corrections have to be applied to proton, gamma and iron showers. Unfortunately, in the analysis of air showers, it is not possible to determine shower type on an event-by-event basis: if we apply this average energy correction to a shower, we make an error of about 5% in the energy determination.

A parameter for SD reconstruction of large air showers is the particle density 1 km from the core of the shower. This parameter, called S(1000), differs from what is commonly used at lower energies, S(600). For the Auger Array, the S(1000) parameter is less dependent on shower-to-shower fluctuations than values of the particle density closer to the core. To obtain the density. To obtain the density, we perform a fit of lateral distribution function to the integrated signals in the tanks as shown in Figure 7. The lateral distribution function is parameterized as a function of distance from shower axis using the function extracted from a fit to data of Haverah Park experiment, and adapted to our energy range:

$$S(r) = kr^{(3.98 - 1.29/\cos + r/4000)} \tag{11}$$

where r is a distance from shower axis in meter. Then, energy is given by

$$E_\circ^{SD} = \frac{S(1000m)}{4.5(2 - 1/cos(\theta)) + 4.5\theta/\pi))} \tag{12}$$

where θ is zenith angle in radian and $S(1000m)$ is density at 1,000 m from core. This conversion relation is obtained by using air shower simulations.

In both case, primary mass cannot be determined on an event-by-event basis, so primary energy is obtained by assuming that primary particles have the average mass for proton and iron. Furthermore, the above relation varies with hadronic interaction models. The energy determination in FD is independent of the models, but depends on fluorescence yield measurements at low energies as well as light scattering and absorption in the atmosphere.

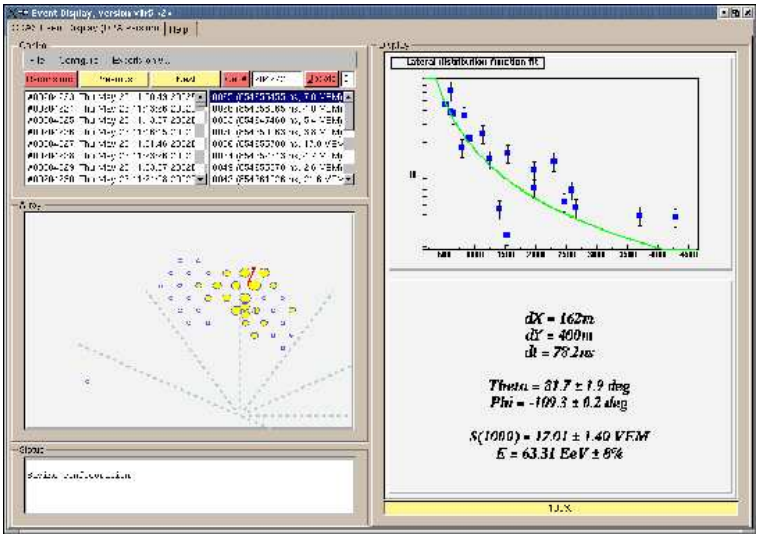

Figure 7. A large event seen in the engineering array. This high zenith angle event hit twenty tanks (two-thirds of the operating tanks at that moment in time). Tanks hit and incoming event direction are indicated on the left. The right portion of the on-line display shows a primitive reconstruction of the shower's lateral distribution function and an estimate of the energy of the shower (63 EeV = 6.3×10^{19} eV).

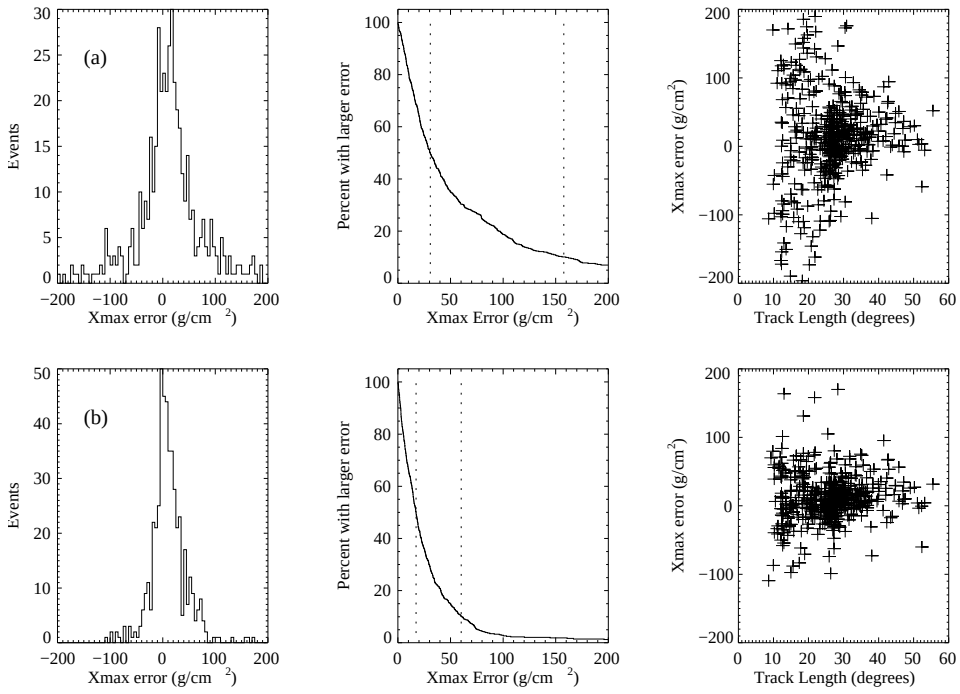

Figure 8. Shown here are the results of profile reconstructions of sample 10^{19} eV air showers analyzed in the (top) pure fluorescence mode and (bottom) hybrid mode of operation. Overall agreement is quite reasonable, errors are significantly reduced in hybrid operation, and the remaining correlations in the errors merely reflect somewhat less than ideal tuning of the analysis.

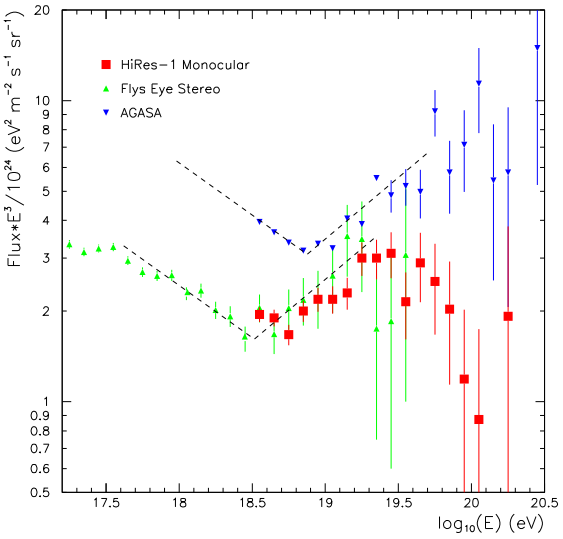

Figure 9. Cosmic ray fluxes obtained by AGASA, Fly's Eye, and HiRes experiments.[12] Curves are to guide the eye only, but might lead one to think that there is both a systematic energy and flux normalization difference between the experimental techniques. Note that the highest energy bins contain only a few events in each experiment.

4. SUMMARY OF RESULTS AND CONCLUSIONS

As previously mentioned, the number of hybrid events is quite small, however, these data allow us to develop reconstruction procedures and assess the performance of the FD and SD acting in concert. Independent groups are working on a full reconstruction of these 77 hybrid events, with some preliminary results which will be shown at the meeting and presented at other forums this year. Surface-only data continues to be collected from the engineering array and as production tanks come online (Fall 2002), the array will grow larger. Science results from this large Southern Hemisphere detector are likely in the near future.

In simulation, see Figure 9, the hybrid reconstruction on the lower set of plots is qualitatively better than the pure (one-eye) fluorescence results. Energy and angular information between the FD and SD seem to agree quite well also, and it is hoped that extensive hybrid data from the production array will address the discrepancy between surface array results (exemplified by AGASA's high energy results[10]) and fluorescence measurements of the highest energy cosmic rays (HiRes results[11]). This discrepancy can be seen in Figure 9.

It seems as though fluorescence measurements consistently yield lower fluxes at very high energy than does the surface array approach. Clearly these two approaches have systematics—for a surface array, one is extrapolating nuclear interaction cross-sections up many orders of magnitude in energy, and for a fluorescence detector, one is typically observing events at several atmospheric attenuation lengths where very good atmospheric information must be available. Though both techniques are mature, there are significant differences in results which have yet to be reconciled.

Looking more closely at the data combined together in Figure 9, HiRes is reporting a total of only two events about 10^{20} eV. This is much less than that predicted by the AGASA spectrum and in fact has lead to some work[13] claiming that the GZK cutoff has now been observed. The handful of super-GZK events are consistent with the soft cut-off and distribution of sources in the universe. There are also claims[14] that this discrepancy can be resolved by reexamining the atmospheric monitoring for fluorescence observations and/or performing new measurements of fluorescence yield. Regardless of cause, the intercalibrated Auger hybrid dataset, once full-scale data taking is underway, is certain to add to, and perhaps resolve, this discussion.

REFERENCES

1. P. Auger, R. Maze, and Grivet-Meyer, *C. R. Acad. Sci.*, Paris, **206** 1721, 1938.
2. A. V. Olinto *Nucl. Phys. Proc. Suppl.* **110** 434, 2002.
3. P. Blasi, R. Dick, and E. W. Kolb *Nucl. Phys. Proc. Suppl.* **110** 494, 2002.
4. L. Anchordoqui, H. Goldberg, S. Reucroft, and J. Swain, *Phys. Rev.* **D64** 123004, 2001.
5. G. Sigl, *Science* **291** 73, 2001.
6. Auger Project Design Report, http://www.auger.org/admin/DesignReport/index.html, 1997.
7. Auger Technical Design Report, http://tdpc01.fnal.gov/auger/org/tdr/index.html, 2002.
8. Other papers in this section of this conference, P. M. Mantsch (4858-11), J. A. Matthews (4858-12), and J. J. Beatty (4858-13).
9. C. Song, *et al*, *Astropart. Phys.*, **14** 7, 2000.
10. N. Sakaki for the AGASA Collaboration, *Proc. 27th Int. Conf. on Cosmic Rays (Hamburg)*, **1** 333, 2001.
11. C. C. H. Jui for the HiRes Collaboration, *Proc. 27th Int. Conf. on Cosmic Rays (Hamburg)*, **1** 354, 2001.
12. R. Abbasi, *et al.*, "Measurement of the Spectrum of UHE Cosmic Rays by the FADC detector of the HiRes experiment", to be submitted for publication, 2002.
13. J. N. Bahcall and E. Waxman, Preprint, **hep-ph/0206217**, 2002.
14. M. Nagano, *et al*, *Proc. 27th Int. Conf. on Cosmic Rays (Hamburg)*, **2** 675, 2001.